Optimization of a Nafion membrane-based system for removal of chloride and fluoride from lunar regolith-derived water

Stephen M. Anthony [a,b,*], Edgardo Santiago-Maldonado [b], James G. Captain [c], Ashtamurthy S. Pawate [a], Paul J.A. Kenis [a]

[a] *Department of Chemical and Biomolecular Engineering, University of Illinois at Urbana-Champaign, Urbana, IL 61801*

[b] *Engineering and Technology Directorate, John F. Kennedy Space Center, National Aeronautics and Space Administration, Kennedy Space Center, FL 32899*

[c] *Applied Science and Technology, QinetiQ North America, Kennedy Space Center, FL 32899*

[*] Corresponding author. Tel. +1 321 867 8433; *E-mail address:* stephen.m.anthony@nasa.gov

Abstract

A long-term human presence in space will require self-sustaining systems capable of producing oxygen and potable water from extraterrestrial sources. Oxygen can be extracted from lunar regolith, and water contaminated with hydrochloric and hydrofluoric acids is produced as an intermediate in this process. We investigated the ability of Nafion proton exchange membranes to remove hydrochloric and hydrofluoric acids from water. The effect of membrane thickness, product stream flow rate, and acid solution temperature and concentration on water flux, acid rejection, and water and acid activity were studied. The conditions that maximized water transport and acid rejection while minimizing resource usage were determined by calculating a figure of merit. Water permeation is highest at high solution temperature and product stream flow rate across thin membranes, while chloride and fluoride permeation are lowest at low acid solution temperature and concentration across thin membranes. The figure of merit varies depending on the starting acid concentration; at low concentration, the figure of merit is highest across a thin membrane, while at high concentration, the figure of merit is highest at low solution temperature. In all cases, the figure of merit increases with increasing product stream flow rate.

Keywords: In Situ Resource Utilization, Water permeation, Chloride permeation, Fluoride permeation, Nafion

1. Introduction

A long-term human presence in space will require systems that do not rely on continuous replenishment of supplies and materials from Earth. The field of *In Situ* Resource Utilization (ISRU) is focused on developing technologies and processes to support self-sustaining systems. The goal of ISRU systems is to use extraterrestrial resources to support activities such as human life-support, material fabrication and repair, and radiation shielding. ISRU resources can potentially be derived from lunar and Martian regolith, and the Martian atmosphere [1].

Permanently-shaded regions of polar craters on the moon are potential sites for exploration and eventual settlement, and lunar regolith is a potential source of oxygen for rocket propellant and life support systems, and raw metal for construction materials [2]. The elemental composition of lunar regolith is very similar to that of terrestrial soil and rock, consisting primarily of oxides of silicon, aluminum, iron, calcium, magnesium, titanium, chromium and manganese [3]. The hydrogen-rich regolith in the polar craters can be exploited by high-temperature reduction of the metal oxides to generate water, which can then be electrolyzed to produce oxygen [4-6].

Water, generated as an intermediate product in the production of oxygen from lunar regolith, contains a number of undesirable contaminants, including hydrochloric and hydrofluoric acids. These acid contaminants are derived from trace amounts of fluoride and chloride present in lunar regolith and are expected to be present in relatively high concentrations in the water thus generated [3]. On Earth, halide contaminants are typically removed from water using consumable adsorbents or processes that require regular replacement or regeneration with large amounts of water or basic solutions [7-20]. These methods are not practical in the lunar environment where resources are extremely limited.

We report the results of our investigation of the feasibility of using a proton exchange membrane as an ISRU alternative for purification of water derived from lunar regolith. Nafion, a commercially-available sulfonated tetrafluoroethylene polymer, is commonly used as a fuel cell proton exchange membrane, and its water permeation properties have been well-studied [21-24]. Due to its high proton and low anion conductivities Nafion is well-suited as a filtration membrane for chloride and fluoride removal [25, 26]. Water diffuses through Nafion via sulfonic acid-lined channels, and anions are rejected via charge exclusion, enabling continuous use of Nafion without the need for regeneration.

In an effort to determine the operating conditions that maximize water transport and acid rejection while minimizing resource usage, the effect of several variables on water flux, acid rejection, and water and acid activity were studied. These results were used to calculate a figure of merit that takes into account the most important parameters needed for developing an *in situ* contaminant removal system for lunar regolith-derived water.

2. Experimental

2.1 Experimental Apparatus

All experiments were performed using the apparatus shown schematically in Fig. 1. The membrane holder was made from two poly(tetrafluoroethylene) (PTFE) plates between which Nafion membranes were secured. The 0.4 cm deep plate cavities were 7.1 cm in diameter yielding a contact area of 39.6 cm^2. The acid solution vessel, acid pump, and all tubing that contacted acid solutions were made from PTFE to prevent corrosion and contamination of the acid solution. A heated water bath circulated through the acid solution vessel to heat it to the desired temperature.

Water, chloride and fluoride permeation were measured for Nafion NR-212, N115 and N1110 membranes (Ion Power) having thicknesses of 51μm, 127 μm and 254 μm respectively, using solutions of 100, 1000 and 10000 parts per million (ppm) by mass of hydrochloric (Fisher) and hydrofluoric (Sigma-Aldrich) acids in deionized water. The acid solutions were pumped at a constant flow rate of approximately 500 mL/min and a temperature varying from 30 to 70 °C through one side of the membrane holder. Dry nitrogen gas was regulated to 50 psig and passed through the other side of the membrane holder at a flow rate that was varied between 1 and 5 L/min by a mass flow controller (MKS). The gas stream was then passed through a bath containing glycol at 0 °C to condense as much of the permeated acid solution as possible. Collection times ranged from 10 min per run at 70 °C to 40 min per run at 30 °C, with a minimum of 500 μL of acid solution collected for each run.

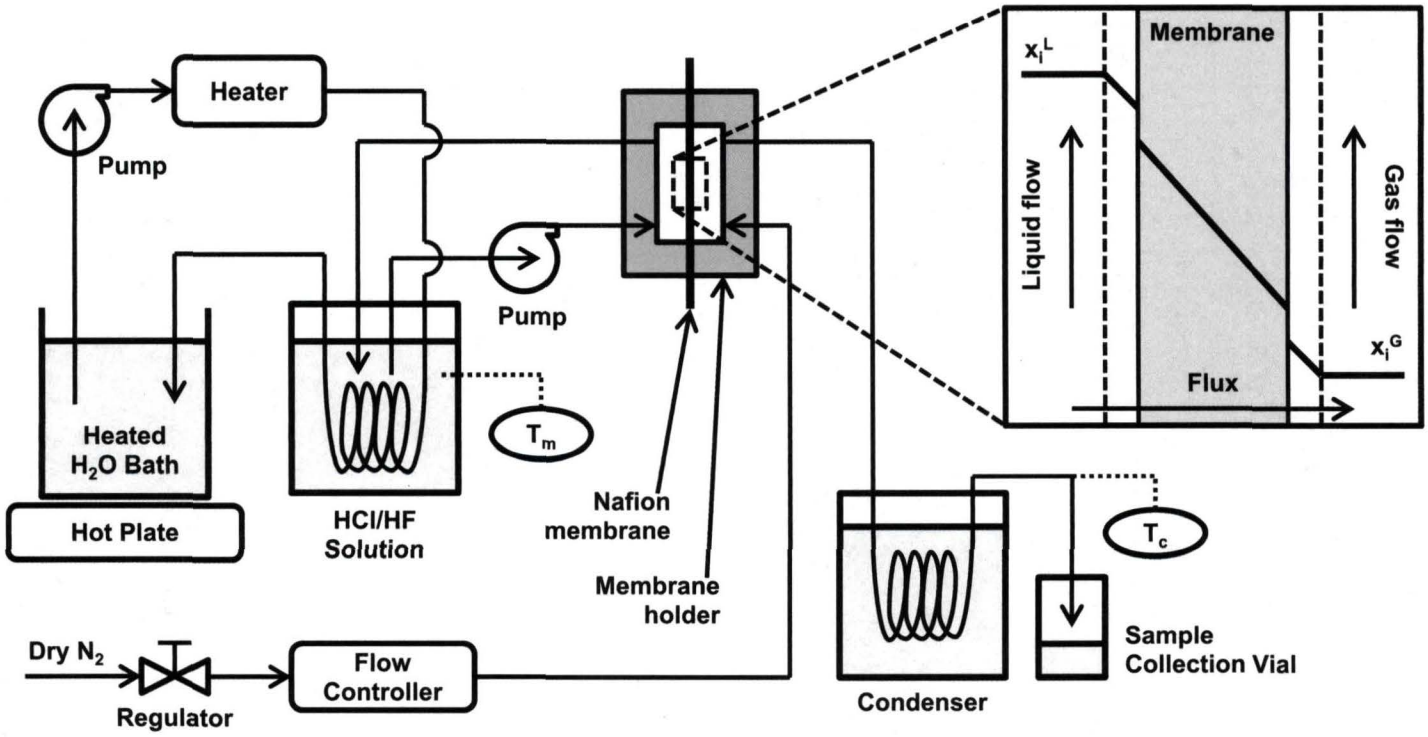

Fig 1. Schematic representation of apparatus to test water flux and acid rejection capabilities of Nafion membranes. Inset (top right): concentration profile of acid solution across membrane cross-section.

2.2 Water Permeation

The molar water flux (N_w) was calculated to reflect the mass of water collected (m), and the theoretical amount of water vapor that was not condensed, based on the vapor pressure (p) of water at the temperatures measured at the membrane (T_m) and the condenser outlet (T_c) as described by Equation 1, where A is the wetted membrane cross-sectional area, and t is the collection time:

$$N_w = \frac{m/18g_{H_2O} \cdot gmol_{H_2O}{}^{-1}}{A \cdot t} \cdot \frac{p(T_m)}{p(T_m) - p(T_c)}$$

(Eq. 1)

The activity of water on the gas side of the membrane ($x_w{}^G$) was also calculated as a function of the water flux and nitrogen flow rate (Q) using Equation 2:

$$x_w^G = \frac{N_w}{N_w + Q \cdot \frac{3.15 \times 10^{-3} g_{N_2} \cdot mL^{-1}}{28 g_{N_2} \cdot gmol_{N_2}{}^{-1}}}$$

(Eq. 2)

2.3 Chloride and Fluoride Permeation

The concentration of chloride and fluoride ions in the collected acid solutions (C_i^G) were measured using the Dionex LC20 Ion Chromatograph, and compared to the starting concentration (C_i^L) to determine the rejection fractions (R_i) of chloride and fluoride using Equation 3:

$$R_i = 1 - \frac{C_i^G}{C_i^L}$$

(Eq. 3)

The activity of chloride and fluoride on the liquid side (x_i^L) gas side (x_i^G) of the membrane were calculated using Equations 4 and 5, M_i is the molecular weight of chloride or fluoride (35 or 19 g·gmol^{-1}, respectively):

$$x_i^L = \frac{C_i^L}{M_i} \cdot \frac{18 g_{H_2O} \cdot gmol_{H_2O}{}^{-1}}{0.998 g_{H_2O} \cdot mL^{-1}}$$

(Eq. 4)

$$x_i^G = \frac{C_i^G \cdot x_w^G}{M_i} \cdot \frac{18 g_{H_2O} \cdot gmol_{H_2O}{}^{-1}}{0.998 g_{H_2O} \cdot mL^{-1}}$$

(Eq. 5)

2.4 Figure of Merit

The molar flux of water, chloride or fluoride (N_i) across the membrane can be expressed in terms of a permeation coefficient (k_i) and the activity of water, chloride or fluoride on the liquid (x_i^L) and gas (x_i^G) sides of the membrane, as shown in Equation 6:

$$N_i = k_i\left(x_i^L - x_i^G\right)$$

(Eq. 6)

In order to determine the conditions that maximize the efficiency of water permeation while minimizing the efficiency of chloride and fluoride permeation, a figure of merit (Z) was defined according to Equation 7. For each sample collected, the permeation coefficients for water (k_w), chloride (k_{Cl}) and fluoride (k_F) were used to calculate the figure of merit:

$$Z = \frac{k_w^2}{k_{Cl} \cdot k_F}$$

(Eq. 7)

3. Results

3.1 Water Permeation

The effect of membrane thickness, liquid-side solution temperature and gas-side nitrogen flow rate on water flux and gas-side water activity are reported in this section. No correlation between acid solution concentration and water flux was observed, so the data collected at different acid solution concentrations were averaged for each solution temperature and gas flow rate.

Water flux across Nafion membranes as a function of solution temperature and gas-side nitrogen flow rate is reported in Fig. 2 for all three membranes tested. The data show that water flux increases with increasing nitrogen flow rate as a logarithmic function as shown in Equation 8, with coefficients a and b shown in Table 1. The water flux increased twofold as the solution temperature increased from 30 to 50 °C, and threefold from 50 to 70 °C. Water flux across the 51 μm membrane was approximately 30% higher than across the 127 μm membrane, and approximately 60% higher than across the 254 μm membrane.

$$N_w = a \cdot \ln Q + b \qquad \text{(Eq. 8)}$$

Table 1: Coefficients of molar water flux versus gas-side nitrogen flow rate equation for varying membrane thickness and liquid-side solution temperature

Membrane Thickness (μm)	**Liquid Temperature (°C)**	***a* x 10^5 (gmol/cm^2·min)**	***b* x 10^5 (gmol/cm^2·min)**
51	30	5	4
	50	10	8
	70	30	30
127	30	3	5
	50	7	10
	70	20	30
254	30	3	3
	50	8	8
	70	20	20

Water activity on the gas side of the membranes as a function of solution temperature and gas-side nitrogen flow rate is reported in Fig. 3 for all three membranes tested. The data show that while water flux increased with increasing nitrogen flow rate, the mole fraction of water on the gas side decreased as an exponential function as shown in Equation 9, with coefficients *c* and *d* shown in Table 2. The gas-side water activity increased threefold as the solution temperature increased from 30 to 50 °C, and threefold from 50 to 70 °C. Gas-side water activity was roughly the same across all membranes at 30 and 50 °C, and decreased slightly with increasing membrane thickness at 70 °C.

$$x_w^G = c \cdot \ln Q + d \qquad \text{(Eq. 9)}$$

Table 2: Coefficients of molar water activity versus gas-side nitrogen flow rate equation for varying membrane thickness and liquid-side solution temperature

Membrane Thickness (μm)	**Liquid Temperature (°C)**	***c* (min/L)**	***d***
51	30	-0.107	.008
	50	-0.102	.028
	70	-0.143	.091
127	30	-0.156	.009
	50	-0.208	.039
	70	-0.207	.092
254	30	-0.160	.008
	50	-0.169	.029
	70	-0.178	.068

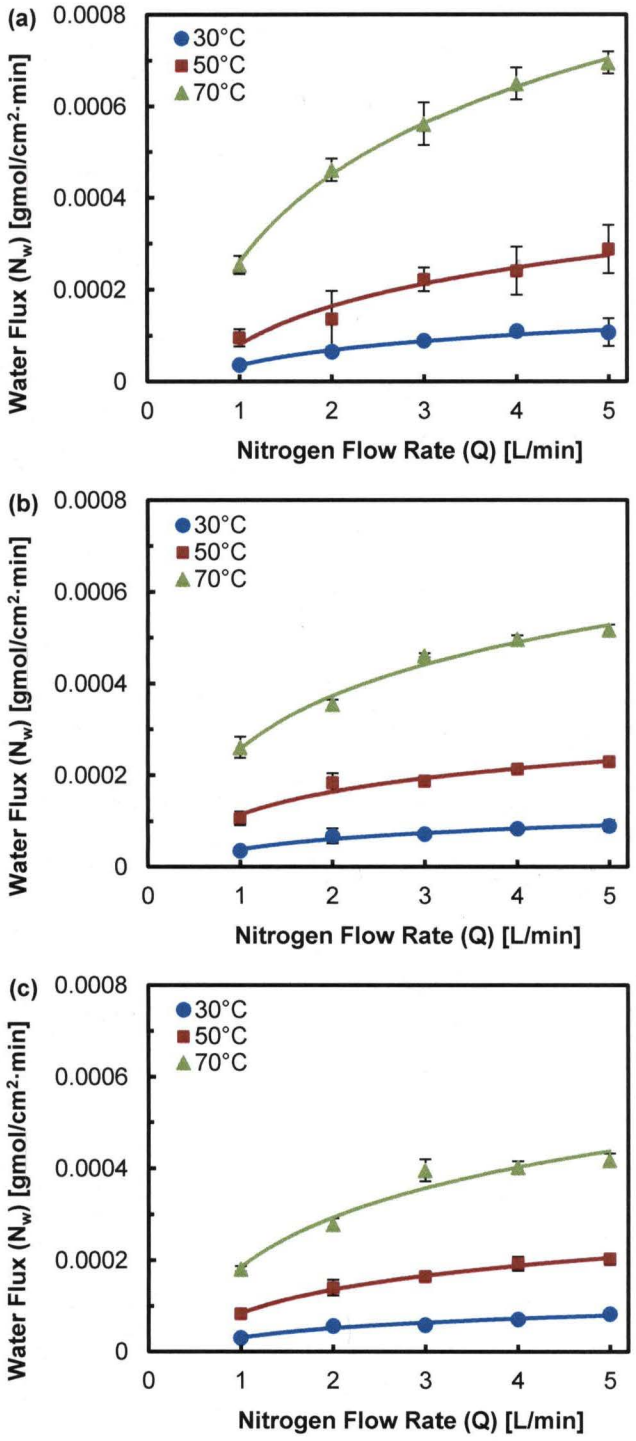

Fig. 2. Water flux across Nafion membranes as a function of nitrogen flow rate and acid solution temperature, with membranes of thickness 51 mm (a), 127 mm (b), and 254 mm (c).

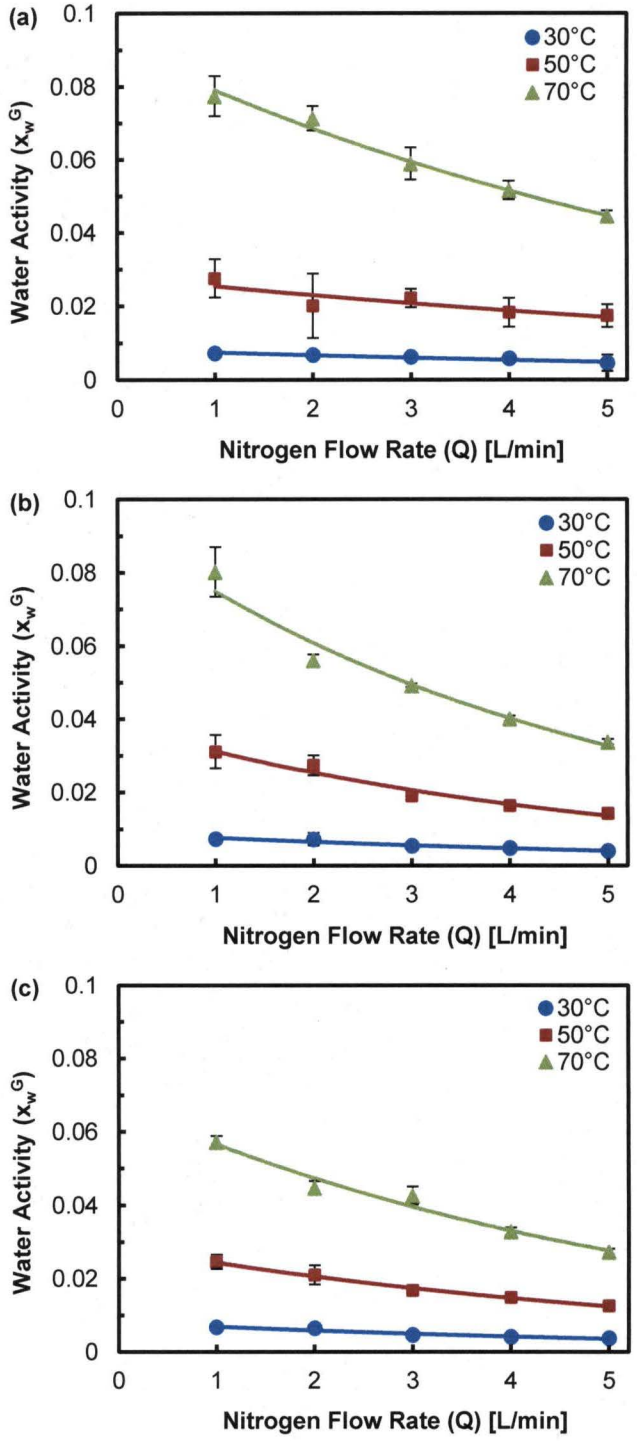

Fig. 3. Water activity on gas side of Nafion membranes as a function of nitrogen flow rate and acid solution temperature, with membranes of thickness 51 mm (a), 127 mm (b), and 254 mm (c).

3.2 Chloride Permeation

The effect of membrane thickness, liquid-side solution temperature and acid concentration on chloride rejection and gas-side chloride activity are reported in this section. No correlation between gas-side nitrogen flow rate and chloride rejection or activity was observed, so the data collected at different flow rates were averaged for each acid solution concentration and temperature.

Chloride rejection as a function of acid solution concentration and temperature is reported in Fig. 4 for all membranes. At acid solution concentrations of 1000 or 10000 ppm, chloride rejection was very high for all membranes tested, at least 96% but most often ranging between 99.0 and 99.9%. At an acid solution concentration of 100 ppm, chloride rejection decreased with increasing membrane thickness. No correlation between chloride rejection and acid solution temperature was observed.

The ratio of gas-side to liquid-side chloride activity as a function of acid solution concentration and temperature is reported in Fig. 5 for all membranes. The chloride activity ratio typically increased by one to two orders of magnitude as the acid solution temperature increased from 30 to 70 °C. For all membrane thicknesses, the chloride activity ratio typically decreased as the acid solution concentration increased from 100 to 10000 ppm. These trends were most pronounced across the 254 μm thick membrane, where at 30 °C the chloride activity ratio decreased by roughly an order of magnitude as the acid solution concentration increased from 100 to 1000 ppm, and decreased by another order of magnitude as the concentration increased to 10000 ppm. The chloride activity ratio also increased by an order of magnitude as the temperature increased from 30 to 70 °C at acid solution concentrations of 100 and 1000 ppm, and increased by over two orders of magnitude at 10000 ppm.

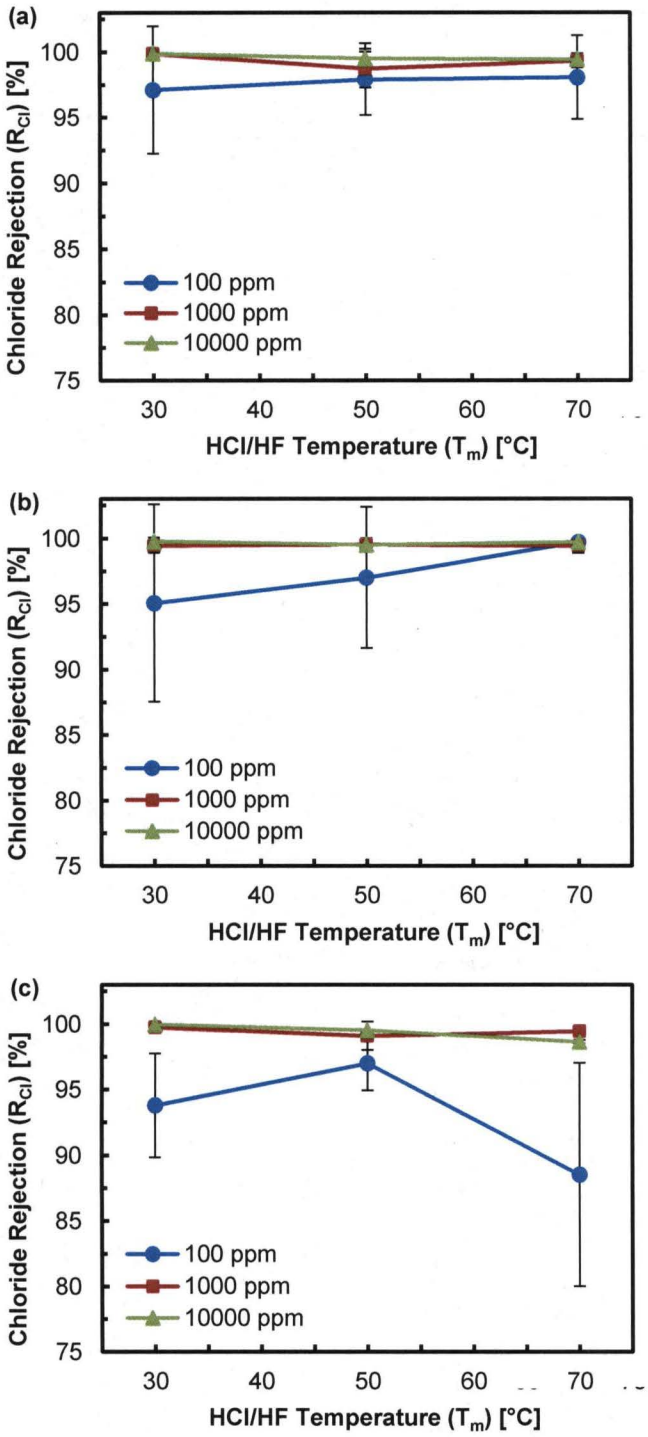

Fig. 4. Chloride rejection by Nafion membranes as a function of HCl/HF solution temperature and concentration, with membranes of thickness 51 mm (a), 127 mm (b), and 254 mm (c).

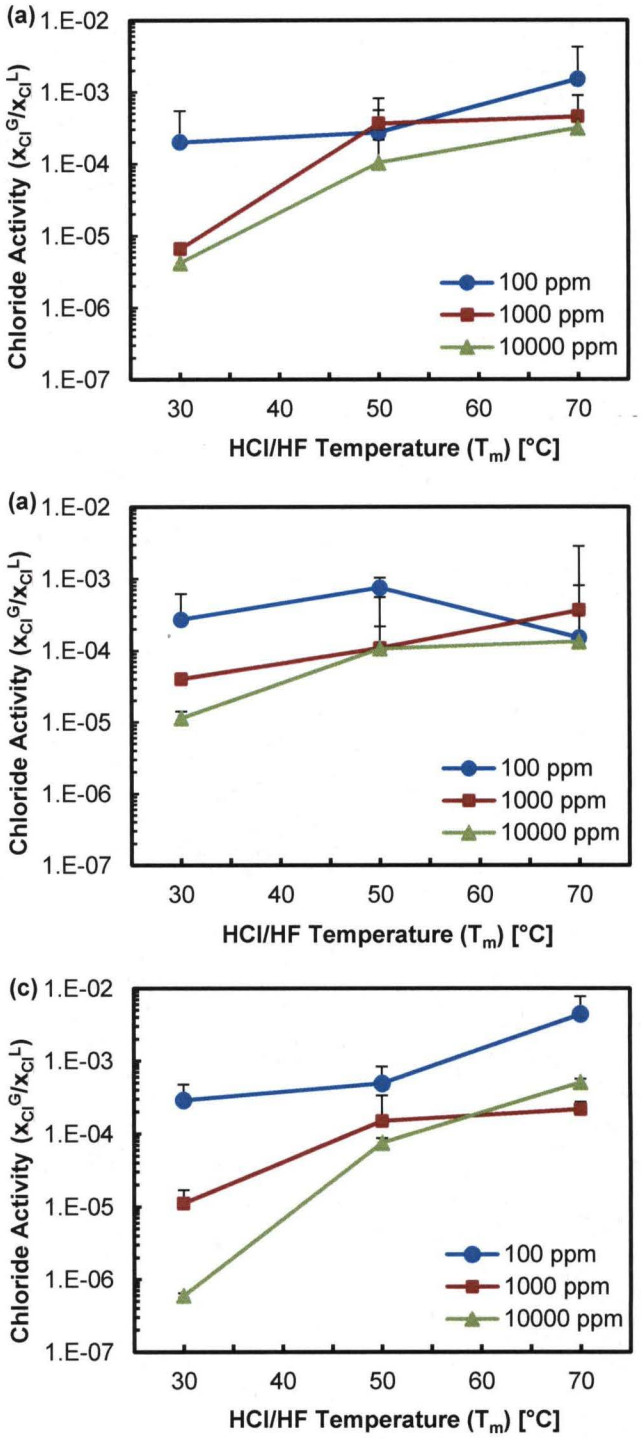

Fig. 5. Ratio of chloride gas-side activity to liquid-side activity as a function of HCl/HF solution temperature and concentration, at membrane thickness of 51 mm (a), 127 mm (b), and 254 mm (c).

3.3 Fluoride Permeation

The effect of membrane thickness, liquid-side solution temperature and acid concentration on fluoride rejection and gas-side fluoride activity are reported in this section. No correlation between gas-side nitrogen flow rate and fluoride rejection or activity was observed, so the data collected at different flow rates were averaged for each acid solution concentration and temperature.

Fluoride rejection as a function of acid solution concentration and temperature is reported in Fig. 6 for all membranes. Fluoride rejection was at least 90% across all membrane thicknesses at a starting solution concentration of 10000 ppm, and was approximately 80% across all membrane thicknesses at 1000 ppm. At an acid solution concentration of 100 ppm, fluoride rejection decreased from approximately 80% across the 51 μm thick membrane to 60% or less across the 127 and 254 μm thick membranes. No correlation between fluoride rejection and acid solution temperature was observed.

The ratio of gas-side to liquid-side fluoride activity as a function of solution concentration and temperature is reported in Fig. 7 for all membranes. In all cases, the fluoride activity ratio increased exponentially with increasing acid solution temperature, increasing by approximately an order of magnitude from 30 to 70 °C. For all membrane thicknesses, the fluoride activity ratio decreased with increasing acid solution concentration. The largest decreases occurred across the 127 and 254 μm thick membranes, where the fluoride activity ratio decreased by approximately an order of magnitude as the acid solution concentration increased from 100 to 10000 ppm at all temperatures.

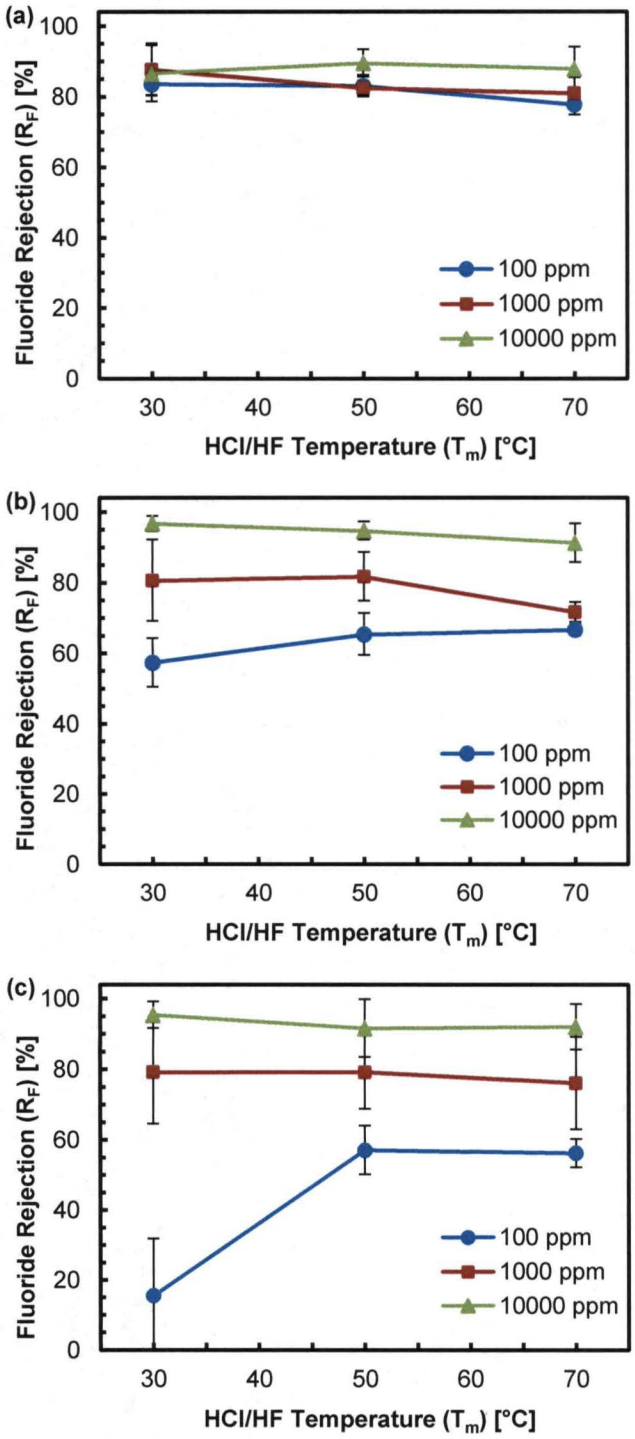

Fig. 6. Fluoride rejection by Nafion membranes as a function of HCl/HF solution temperature and concentration, with membranes of thickness 51 mm (a), 127 mm (b), and 254 mm (c).

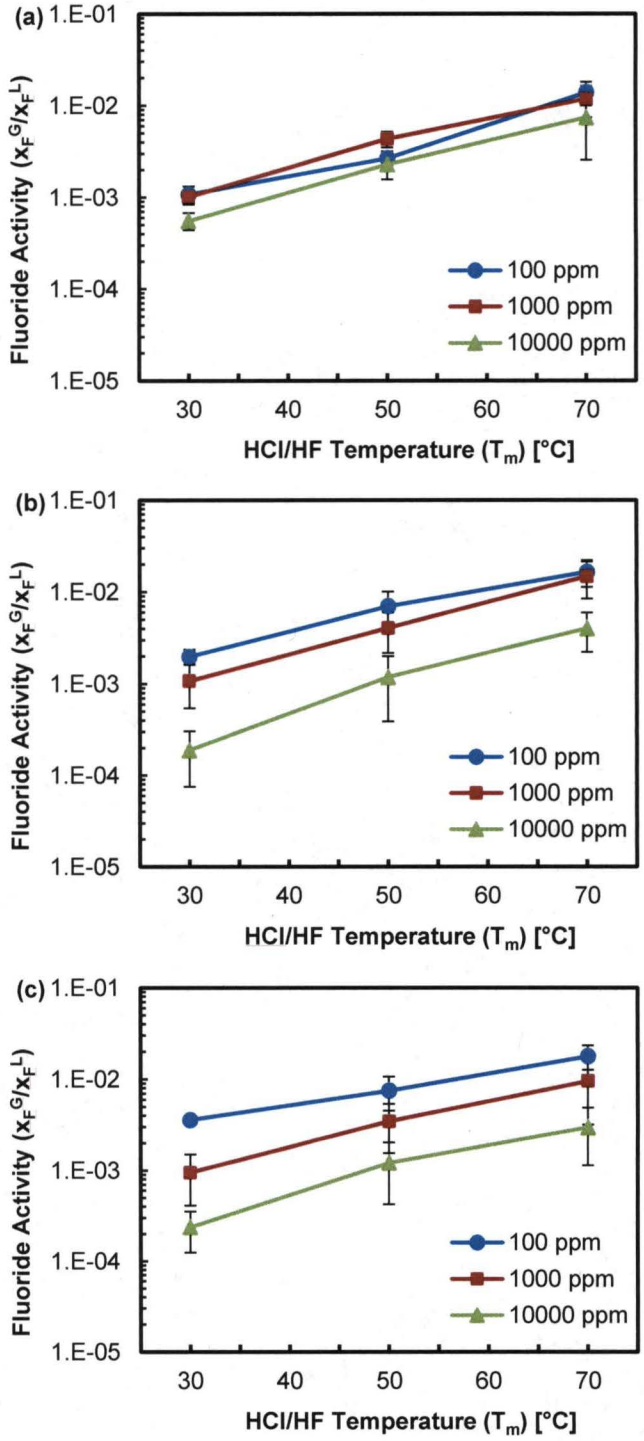

Fig. 7. Ratio of fluoride gas-side activity to liquid-side activity as a function of HCl/HF solution temperature and concentration, at membrane thickness of 51 mm (a), 127 mm (b), and 254 mm (c).

3.4 Figure of Merit

The figure of merit as a function of solution concentration and temperature, and gas-side nitrogen flow rate is reported at acid solution concentrations of 100 ppm (Fig. 8), 1000 ppm (Fig. 9), and 10000 ppm (Fig. 10). For each sample collected, the calculated figure of merit was normalized to the maximum value for that acid solution concentration.

At an acid solution concentration of 100 ppm, the figure of merit increased with increasing gas flow rate and decreased with increasing membrane thickness. No relationship between acid solution temperature and the figure of merit was observed. At an acid solution concentration of 1000 ppm, the figure of merit increased with increasing gas flow rate, and decreased with increasing membrane thickness and acid solution temperature. At an acid solution concentration of 10000 ppm, the figure of merit increased with increasing gas flow rate and decreased with increasing acid solution temperature. No relationship between membrane thickness and the figure of merit was observed.

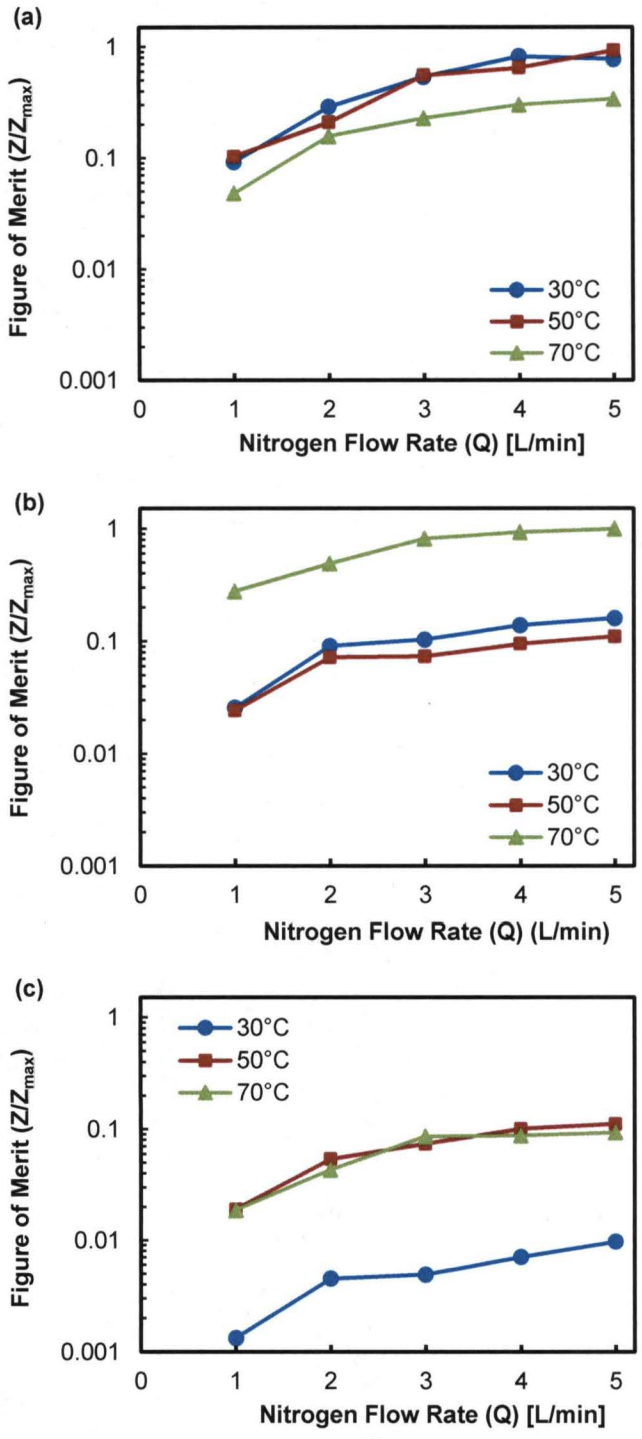

Fig. 8. Normalized figure of merit as a function of gas-side nitrogen flow rate and liquid-side acid solution temperature, with acid solution concentration of 100 ppm and membrane thicknesses of 51 μm (a), 127 μm (b), and 254 μm (c).

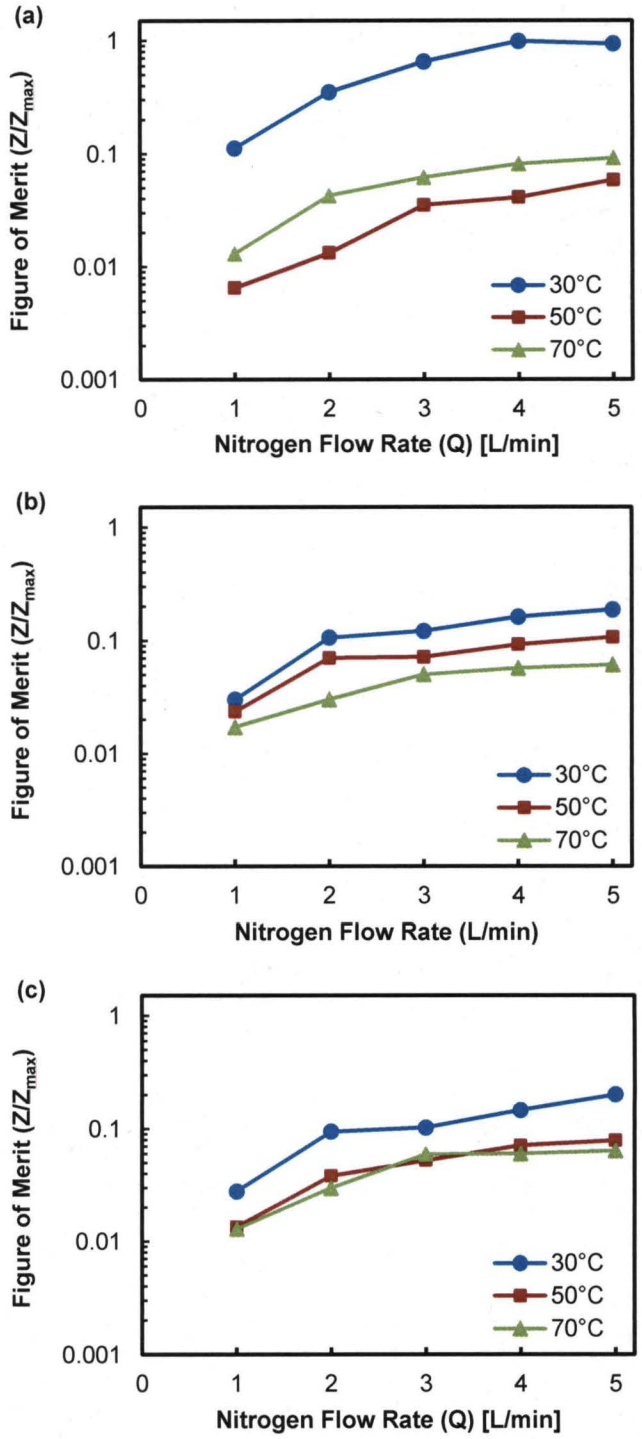

Fig. 9. Normalized figure of merit as a function of gas-side nitrogen flow rate and liquid-side acid solution temperature, with acid solution concentration of 1000 ppm and membrane thicknesses of 51 μm (a), 127 μm (b), and 254 μm (c).

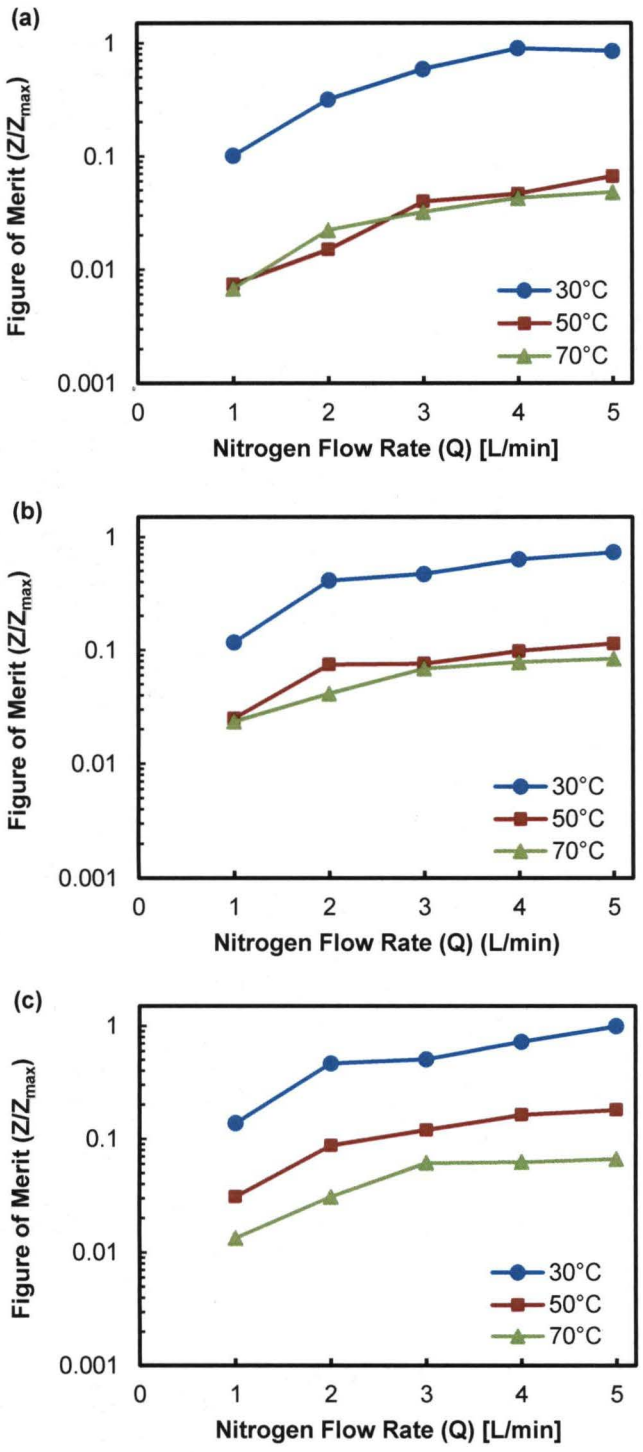

Fig. 10. Normalized figure of merit as a function of gas-side nitrogen flow rate and liquid-side acid solution temperature, with acid solution concentration of 10000 ppm and membrane thicknesses of 51 μm (a), 127 μm (b), and 254 μm (c).

4. Discussion

4.1 Water Permeation

Water flux (N_w) across Nafion membranes and gas-side water activity (x_w^G) are highly dependent on water temperature and gas flow rate, while membrane thickness has a much smaller effect. This is consistent with previous studies [22]. While water flux increased significantly with increasing gas flow rate, the gas-side water activity also decreased significantly. It is possible that higher gas flow rates cool the gas side of the membrane, decreasing the water permeation efficiency. The water permeation coefficient (k_w) takes into account both trends.

4.2 Chloride and Fluoride Permeation

The high rejection and low gas-side activity of chloride and fluoride can be attributed to charge exclusion. Briefly, the water channels in Nafion membranes in acid form are lined with sulfonic acid end groups, and when the membrane is soaked in water, protons tend to diffuse out, leaving a negative potential in the water channels [26, 27]. As a strong acid ($pK_a \sim 7$), HCl fully dissociates in water, and the negative potential of the membrane channels inhibits diffusion of chloride across the membrane. Since HF is a weak acid ($pK_a = 3.17$) [28], fluoride rejection is expected to be lower than chloride rejection, as permeation of undissociated HF is not as inhibited by the negative potential of the water channels as dissociated anions.

The tendency for chloride and fluoride rejection to increase with increasing temperature may be due to an increase in proton diffusion out of the water channels as the water channels swell with increasing temperature, thereby increasing the negative potential of the water channels and further inhibiting anion diffusion. Similarly, the tendency for anion rejection to decrease with increasing membrane thickness may be due to less efficient proton diffusion out of the water channels of thicker membranes, which would decrease the negative potential of the water channels and promote anion diffusion.

Fluoride rejection increases with increasing acid solution concentration. A similar but less pronounced trend is observed with chloride. If fluoride rejection was governed solely by dissociation equilibrium, however, fluoride rejection would be expected to increase with decreasing acid solution concentration, as the calculated mole fraction of dissociated fluoride increases from 0.036 to 0.110 to 0.306 as HF solution concentration decreases from 10000 ppm to 1000 ppm to 100 ppm. Previous studies have shown that fluoride permeation across Nafion membranes increases significantly with decreasing pH [26]. Solutions of 100 ppm, 1000 ppm and 10000 ppm HF have pH values of 1.74, 2.26 and 2.81, respectively, while solutions of 100 ppm, 1000 ppm and 10000 ppm HCl/HF have pH values of 0.53, 1.48 and 2.37, respectively. The reduced pH due to the presence of chloride in the acid solution, which is particularly significant at lower concentrations, may account for this observation.

While anion flux (N_{Cl}, N_F), which is inversely proportional to chloride rejection, decreases with increasing temperature, the gas-side anion activity (x_{Cl}^G, x_F^G), essentially the mole fraction of chloride or fluoride in the gas stream, increases. This is likely due to the increased water activity at higher temperatures. The anion permeation coefficients (k_{Cl}, k_F) account for both trends.

4.3 Figure of Merit

In all cases, the figure of merit increased with increasing gas flow rate, because the water permeation coefficient increased with increasing gas flow rate while the anion permeation coefficients were not affected by gas flow rate.

At the two lowest acid solution concentration (Fig. 8, Fig. 9), the figure of merit is highest across the thinnest membrane. The effect of membrane thickness on the figure of merit is due to the significant decrease in both chloride and fluoride rejection with increasing membrane thickness at lower acid solution concentrations, coupled with the decrease in water flux with increasing membrane thickness across all acid solution concentrations.

The figure of merit at the highest acid solution concentration (Fig. 10) shows that membrane thickness does not affect the figure of merit. Chloride and fluoride activity decrease with increasing membrane thickness at the highest acid solution concentration, negating the similar decrease in water flux.

The figure of merit is highest at the lowest acid solution temperature, particularly for thinner membranes and at higher acid solution concentrations. The figure of merit tends to increase with decreasing temperature because the product of the anion permeation coefficients (particularly that of chloride) decreases at a greater rate than the water permeation coefficient.

5. Conclusions

The permeation of water, fluoride and chloride for solutions of hydrochloric and hydrofluoric acids across Nafion membranes have been determined as a function of membrane thickness, gas flow rate, and acid solution temperature and concentration. Water permeation is maximized across thinner membranes at higher temperatures and gas flow rates. Chloride and fluoride permeation are minimized across thinner membranes at lower acid solution temperatures and concentrations.

A figure of merit was developed to determine the conditions under which water permeation is maximized while chloride and fluoride permeation are minimized. At all acid solution concentrations, the figure of merit increased with increasing gas flow rate. At low acid solution concentrations (on the order of 100 ppm HCl/HF), membrane thickness had the greatest effect on the figure of merit, which increased with decreasing thickness. At high acid solution concentrations (on the order of 10000 ppm), acid solution temperature had the greatest effect on the figure of merit, which increased with decreasing temperature. The figure of merit is a useful tool for optimizing the operating conditions of an ISRU water purification system.

Acknowledgement

The authors thank Bill Larson, ISRU Project Manager at Kennedy Space Center, and the Kennedy Graduate Fellowship Program for its support of this work.

Nomenclature

A	membrane contact area [cm^2]
C_i^G	gas-side concentration of i in water [ppm]
C_i^L	liquid-side concentration of i in water [ppm]
m	mass of acid solution collected [g]
N_i	molar flux of i [$gmol/cm^2 \cdot min$]
$p(T_i)$	vapor pressure of water at temperature T_i [torr]
Q	gas flow rate [L/min]
R_i	membrane rejection fraction of i
t	sample collection time [min]
T_i	temperature measurement at location i [°C]
x_i^G	gas-side activity of i
x_i^L	liquid-side activity of i
Z	figure of merit
Z_{max}	maximum figure of merit at specific acid solution concentration

References

[1] A. Torasso, ISRU technologies and sustainable space exploration, AIAA 58th International Astronautical Congress (2007) 7115-7127.

[2] E. Vallerani, G.G. Ori, A. Della Torre, M. Grasso, G.P. Guizzo, I. Vukman, ISRU: Perspectives for lunar development, AIAA 57th International Astronautical Congress (2006) 1748-1762.

[3] C.M. Schrader, D.L. Rickman, C.A. McLemore, J.C. Fikes, Lunar Regolith Simulant User's Guide, NASA/TM-2010-216446.

[4] U. Hedge, R. Balasubramaniam, S. Gokoglu, Analysis of thermal and reaction times for hydrogen reduction of lunar regolith, Space Technology and Applications International Forum (2008) 195-202.

[5] S. Maurice, W.C. Feldman, D.J. Lawrence, O. Gasnault, R.C. Elphic, S. Chevrel, Distribution of hydrogen at the surface of the moon, Lunar and Planetary Science 34 (2003) 1867.

[6] B. Ruiz, J. Diaz, B. Blair, M.B. Duke, Is extraction of methane, hydrogen and oxygen from the lunar regolith economically feasible? Space Technology and Applications International Forum (2004) 984-991.

[7] M. Arda, E. Orhan, O. Arar, M. Yuksel, N. Kabay, Removal of fluoride from geothermal water by electrodialysis, Separation Science and Technology 44 (2009) 841-853.

[8] M. Behbahani, M.R. Alavi Moghaddam, M. Arami, Techno-economical evaluation of fluoride removal by electrocoagulation process: Optimization through response surface methodology, Desalination 271 (2011) 209-218.

[9] S. Deng,H. Liu, W. Zhou, J. Huang, G. Yu, Mn-Ce oxide as a high-capacity adsorbent for fluoride removal from water, Journal of Hazardous Materials 186 (2011) 1360-1366.

[10] C.K. Diawara, S.M. Lo, M. Rumeau, M. Pontie, O. Sarr, A phenomenological mass transfer approach in nanofiltration of halide ions for a selective defluorination of brackish drinking water, Journal of Membrane Science 219 (2003) 103-112.

[11] X. Dou, Y. Zhang, H. Wang, T. Wang, Y. Wang, Performance of granular zirconium-iron oxide in the removal of fluoride from drinking water, Water Research 45 (2011) 3571-3578.

[12] N.C. Lu, J.C. Liu, Removal of phosphate and fluoride from wastewater by a hybrid precipitation-microfiltration process, Separation and Purification Technology 74 (2010) 329-335.

[13] M. Malakootian, A. Fatehizadeh, N. Yousefi, M. Ahmadian, M. Moosazadeh, Fluoride removal using regenerated spent bleaching earth (RSBE) from groundwater: Case study on Kuhbonan water, Desalination 277 (2011) 244-249.

[14] P. Miretzky, A.F. Cirelli, Fluoride removal from drinking water by chitosan derivatives and composites: A review, Journal of Fluorine Chemistry 132 (2011) 231-240.

[15] M. Mohapatra, S. Anand, B.K. Mishra, D.E. Giles, P. Singh, Review of fluoride removal from drinking water, Journal of Environmental Management 91 (2009) 67-77.

[16] G. Patel, U. Pal, S. Menon, Removal of fluoride from aqueous solution by CaO nanoparticles, Separation Science and Technology 44 (2009) 2806-2826.

[17] H. Paudyal, B. Pangeni, K, Inoue, H. Kawakita, K. Ohto, H. Harada, S. Alam, Adsorptive removal of fluoride from aqueous solution using orange waste loaded with multi-valent metal ions, Journal of Hazardous Materials 192 (2011) 676-682.

[18] M. Sanchez-Polo, J. Rivera-Utrilla, E. Salhi, U. von Gunten, Ag-doped carbon aerogels for removing halide ions in water treatment, Water Research 41 (2007) 1031-1037.

[19] Y. Sun, Q. Fang, J. Dong, X. Cheng, J. Xu, Removal of fluoride from drinking water by natural stilbite zeolite modified with Fe(III), Desalination 277 (2011) 121-127.

[20] F. Treptow, A. Jungbauer, K. Hellgradt, Halide diffusion in polyaniline membranes, Journal of Membrane Science 270 (2006) 115-122.

[21] G. Alberti, R. Narducci, M. Sgnappa, Effects of hydrothermal/thermal treatments on the water-uptake of Nafion membranes and relations with changes of conformation, counter-elastic force and tensile modulus of the matrix, Journal of Power Sources 178 (2008) 575-583.

[22] P.W. Majsztrik, M.B. Satterfield, A.B. Bocarsly, J.B. Benziger, Water sorption, desorption and transport in Nafion membranes, Journal of Membrane Science 301 (2007) 93-106.

[23] K. Schmidt-Rohr, Q. Chen, Parallel cylindrical water nanochannels in Nafion fuel-cell membranes, Nature Materials 7 (2008) 75-83.

[24] X. Ye, M.D. LeVan, Water transport properties of Nafion membranes Part I. Single-tube membrane module for air drying, Journal of Membrane Science 221 (2003) 147-161.

[25] J. Ramkumar, E.K. Unnkrishnan, B. Maiti, P.K. Mathur, Facilitated transport of halides through Nafion ionomer membrane modified with lanthanide complexes, Journal of Membrane Science 141 (1998) 283-288.

[26] E.K. Unnikrishnan, S.D. Kumar, B. Maiti, Permeation of inorganic anions through Nafion ionomer membrane, Journal of Membrane Science 137 (1997) 133-137.

[27] F. Helffierich, Ion Exchange, McGraw-Hill (1962), 134-147.

[28] L.G. Wade, Organic Chemistry, 4th Ed., Prentice-Hall (1999), 25.